
Article:
Cao, Y. orcid.org/0000-0002-6353-7660, Blain, T. orcid.org/0000-0002-7974-7355, Li, L. orcid.org/0000-0003-3184-7434 et al. (4 more authors) (2024) GaAsSb/AlGaAsSb avalanche photodiode with high gain-linearity. IEEE Transactions on Electron Devices, 71 (10). pp. 6161-6165. ISSN 0018-9383

https://doi.org/10.1109/ted.2024.3440279

GaAsSb / AlGaAsSb avalanche photodiode with high gain-linearity

Y. Cao, T. Blain, L. Li, J. D. Veitch, X. D. Collins, J. S. Ng, *Member, IEEE,* and C. H. Tan, *Senior Member, IEEE*

***Abstract*—Avalanche photodiodes (APDs) are widely used in near-infrared optical receivers to detect weak and/or high-speed optical signals. Emerging high-order optical signal modulation formats require the APD's photocurrents to vary linearly with the signal power. There is however a lack of comprehensive understanding of the linearity of APD's photocurrent and gain versus optical power characteristics underpinned by experimental results. An experimental study was carried out on the linearity of near-infrared APD's photocurrent and avalanche gain with optical signal power, covering a wide range of optical power and APD's operating voltage. The work utilized thin 200 nm $Al_{0.85}Ga_{0.15}As_{0.56}Sb_{0.44}$ avalanche region, exploiting their excellent temperature stability compared to thick structures and other commonly used avalanche materials. Three types of linearity behaviors were identified and explained: (i) around the punch-through voltage, (ii) higher reverse bias and moderate gains, and (iii) close to the breakdown voltage and large gains. The best linearity performance, tested under optical power from 0.08 to 750 μW, was achieved under high reverse bias (>18 V) but with moderate gain (< 10). Our findings of linearity performance are also applicable to near-infrared APDs with other avalanche materials. Furthermore, $Al_{0.85}Ga_{0.15}As_{0.56}Sb_{0.44}$-based APDs exhibit better linearity performance compared to a commercial non-$Al_{0.85}Ga_{0.15}As_{0.56}Sb_{0.44}$ APD. At a gain of 10, a 10% attenuation was observed at the output current of 34 μA in the commercial APD compared to 670 μA (20 times higher) in our APD, suggesting the potential of our detector for optical communication links utilizing high-order signal modulation formats. The data reported in this article is available from the ORDA digital repository (https://figshare.com/s/34f0f27e42de168c5c41).**

***Index Terms*—AlGaAsSb, GaAsSb, avalanche photodiode, high temperature stability, linearity, high-order modulation.**

I. Introduction

APDs sensitive to 1310, and 1550 nm wavelength photons are widely used in high-speed optical communication links and optical receivers of high sensitivity. Compared to conventional photodiodes, APDs provide internal gain, amplifying the signal and improving the optical receiver's sensitivity. High-order signal modulation formats offer a significant increase in the bandwidth and the overall transmission rate of the link [1]. However, implementation of such modulation formats is only viable when the APDs can meet the additional demand of good linearity in the photocurrent-optical signal power characteristics [2].

At low optical power, APDs tend to exhibit good linearity of photocurrent, I_{ph}, versus optical power characteristics but the linearity degrades under high optical power [3]. This is attributed to the space-charge effect(s) and general temperature dependence of avalanche gain [4]. Existing works mainly reported improved APD's linearity through APD design, such as using a hybrid absorber instead of the fully depleted absorber [1] and dual-carrier injection structure [4]. Simulation works on APDs emphasized the importance of the hybrid absorber layer, optimal charge sheet layer, and avalanche layer thickness in improving the APDs' linearity [5], [6]. There is however a lack of comprehensive understanding of space-charge effect(s) in APDs underpinned by detailed data and analyses of the dependence of an APD's photocurrent and gain on optical signal power. This is unsurprising because, as the optical signal power increases, the APD is subjected to a higher temperature than intended, which could cause a noticeable variation in the APD's gain. Thus, it can be difficult to experimentally separate the effects of optical signal power on the APD's photocurrent from those on the temperature dependence of the APD's gain.

A simulation-based approach to gain an understanding of how APD's linearity of photocurrent versus optical power is also unlikely to yield useful knowledge. Such studies require simulation models with sufficient band structure and carrier scattering details at high energy, where impact ionization (the mechanism behind avalanche gain) takes place. This level of detail is not available in the range of established simulation models for predicting APD's gain versus reverse bias, and excess noise factors versus gain [7], [8], [9]. Furthermore, most models do not have accurate parameters to simulate temperature dependence of breakdown voltage.

Separate Absorption Multiplication Avalanche Photodiode (SAM-APD) utilizing $Al_{0.85}Ga_{0.15}As_{0.56}Sb_{0.44}$ (referred to as AlGaAsSb hereafter) avalanche regions [10], [11] for 1550 nm wavelength detection have been reported to exhibit avalanche gain characteristics with very weak temperature dependence. They use either an $In_{0.53}Ga_{0.47}As$ (referred to as InGaAs hereafter) [12], [13] or a $GaAs_{0.52}Sb_{0.48}$ (referred to as GaAsSb hereafter) absorber [11], [14]. The thin AlGaAsSb SAM-APD shows a temperature coefficient of breakdown voltage, C_{bd}, of ~ 4.3 ± 0.3 mV/K [14], which is lower than the thick AlGaAsSb SAM-APD [11] and considerably lower than typical values of InGaAs/InP APDs (50 - 150 mV/K [15], [16], [17]) or InGaAs/InAlAs APDs (15 - 40 mV/K [17], [18], [19]), which were used in prior APD linearity studies [1], [4], [5], [6]. Hence, by using an AlGaAsSb SAM-APD with a thin avalanche region (high temperature stability of avalanche gain), it is possible to obtain reliable experimental data on how optical signal power affects the APD's photocurrent, without the complications of noticeable APD's gain variation with temperature.

Manuscript received June 04, 2024; revised July 30, 2024; accepted August xx, 2024. This work was supported by the UK-Engineering and Physical Sciences Research Council grants (EP/N020715/1 and EP/K001469/1).

Y. Cao was with the Department of Electronic and Electrical Engineering, University of Sheffield, Sheffield S1 3JD, UK (email: ycao51@sheffield.ac.uk). He is now with Phlux Technology, Sheffield, S1 4DP, UK (email: ye.cao@phluxtechnology.com).

T. Blain, L. Li, J. D. Veitch, J. S. Ng and C. H. Tan (corresponding author) are with the Department of Electronic and Electrical Engineering, The University of Sheffield, Sheffield S1 3JD, U.K. (e-mail: t.blain@sheffield.ac.uk; lli52@sheffield.ac.uk; j.d.veitch@sheffield.ac.uk; j.s.ng@sheffield.ac.uk; c.h.tan@sheffield.ac.uk).

X. D. Collins is with the Phlux Technology, Sheffield, S1 4DP, UK (email: xiao.collins@phluxtechnology.com).

AlGaAsSb-based SAM-APDs [10], [11], [12] exhibit excess noise performance superior to that of commercial SAM-APDs [20]. This was recently confirmed by an extremely low Noise-Equivalent-Power value of 69 fW/Hz$^{1/2}$ (at a gain of 106 and 215 MHz system bandwidth) from an InGaAs/AlGaAsSb SAM-APD [12]. Avalanche gain and excess noise factor have been the focus of recent reports on AlGaAsSb-based SAM-APDs, but their linearity performance in photocurrent-optical signal power characteristics has not been reported. In this work, we present a detailed experimental study of the linearity of AlGaAsSb-based SAM-APD's photocurrent and avalanche gain with optical signal power, covering a wide range of optical power and APD's operating voltage. We have used a thin AlGaAsSb avalanche region to minimize the effect of temperature on gain variation, such that the effect of optical power can be better understood.

II. Experimental Details

The SAM-APD used in this work is shown schematically in Fig. 1 (a) and (b). It uses a hybrid absorber, which has been shown to improve linearity in uni-travelling-carrier photodiode [20]. The 1.38 µm thick GaAsSb hybrid absorber consists of a p^{++}-doped GaAsSb layer, a p^{+}-doped GaAsSb layer, and a neutral GaAsSb layer. The bandgap grading between the GaAsSb absorber and the 200 nm AlGaAsSb avalanche layer is implemented using three $Al_{1-x}Ga_xAs_{0.56}Sb_{0.44}$ layers (with a total thickness of 88 nm) with x = 0.2, 0.5, and 0.8.

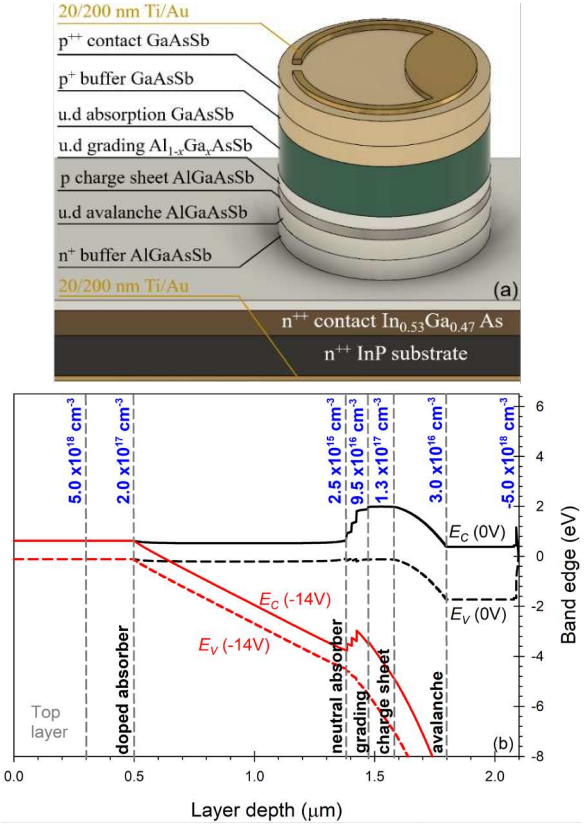

Fig. 1. (a) Schematic of GaAsSb/AlGaAsSb SAM-APD. (b) Energy band diagrams of the SAM-APD at 0 and -14 V modelled by NextNano.

Circular mesa APDs with diameters of 400, 200, 100, and 50 µm were fabricated from the wafer using conventional photolithography and wet chemical etching. Annular top and solid back Ti/Au (20/200 nm) contacts were deposited using thermal evaporation. A phosphoric-based solution was used in the etching process, etching down to the n^{+} AlGaAsSb cladding layer. A 1.5 µm thick SU-8 was spun on the mesa diodes, acting as a passivation layer to prevent oxidation and improve surface condition. The extracted wafer details from capacitance-voltage fitting results [10] (e.g. doping density and layer thickness) are also included in Fig. 1 (b).

The measurements focus on APDs with a diameter of 200 µm, because they offer robust I_{ph} measurements with low optical signal power (dark currents are sufficiently low) and ease of optical alignment. All measurements were performed at room temperature. Reverse dark current versus bias measurements were carried out to identify/confirm the APD under test was functioning. Data of photocurrent versus reverse bias were obtained as a function of optical signal power from three APDs, to yield reliable mean values for each set of experimental conditions. Avalanche gain, M, versus reverse bias data were extracted from these I_{ph} data, by dividing the I_{ph} values by the I_{ph} value at the punch-through voltage. It was assumed that M = 1.30 at -14 V [10]. Responsivity data were also obtained from the I_{ph} data, using the ratio of I_{ph} to optical signal power.

Phase-sensitive detection was employed in the I_{ph} versus reverse bias measurements, ensuring that our I_{ph} and gain data are unaffected by reverse dark currents, particularly when optical signal power is low. This was implemented by using (i) a modulated 1550 nm wavelength laser to provide the optical signal and (ii) a lock-in amplifier to measure the modulated APD's photocurrent in response to the optical power. The optical illumination from the laser was attenuated by a variable optical attenuator before being delivered via a single-mode fiber to the APDs under test, facilitating straightforward adjustment of the optical signal power from -51 to -1.23 dBm. The values of optical signal power falling on our APD were experimentally confirmed using a commercial InGaAs photodiode (also 200 µm diameter) with a known responsivity at 1550 nm wavelength. The optical power values used for our APDs included a 32% reflection loss at the air/semiconductor interface. The optical reflection loss was obtained from $\left(\frac{n_2-n_1}{n_2+n_1}\right)^2$, where n_2 is the refractive index of GaAsSb (3.64 from interpolation of GaSb and GaAs values [21]) and n_1 is the refractive index of air (1.0).

Fitting linear regressions to data of I_{ph} versus optical power at low optical power (I_{ph} <10 µA) yielded the expected ideal photocurrent, I_{ideal}, versus optical power characteristics. These were used for evaluating the linearity photocurrent attenuation under high optical power and an example of fitting is shown in Fig. 2. Values of coefficient of determination, termed R^2, from these fittings to our data at -18 to -48 V all exceed 0.99, indicating I_{ph} depends linearly on optical power over the fitted range.

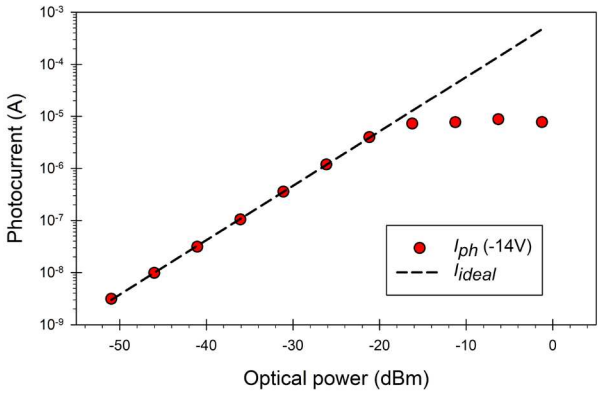

Fig. 2. Example linear regression fitting to data of photocurrent versus optical power from a 200 µm diameter AlGaAsSb-based SAM-APD at -14 V to obtain the ideal photocurrent, I_{ideal}.

III. Results

Photocurrents induced by input optical powers of -30.5, -19.2, and -5.4 dBm are compared to the dark current in Fig. 3 (a). The dark current is dominated by surface leakage mechanisms at reverse biases below -48 V [10]. A rapid increase in the dark current above -48 V is attributed to avalanche breakdown. For a given reverse bias, as the photocurrent increases with optical power, as expected for APDs. All the photocurrent versus reverse bias characteristics exhibit step increases in photocurrent ~ -14 V, the punch-through voltage of these APDs, which varies with optical power at a rate of ~ 79.45 mV/dBm over the range of optical power used. For this work, we use -14 V as the punch-through voltage of these APDs (obtained under a -19.2 dBm (12 µW) laser illumination).

Responsivity and avalanche gain versus reverse bias characteristics are shown in Fig. 3 (b). The data presented are mean values (from three APDs) with error bars representing the standard deviations. At -14 V, the responsivity is 0.5 A/W. As reverse bias increases, responsivity reaches as high as 50 A/W, corresponding to M = 100 at -49.5 V.

Fig. 4 (a) shows I_{ph} versus optical power from -51 to -1.25 dBm (corresponding to 0.08 to 750 µW) as a function of reverse bias. It can be observed that the linearity of photocurrent versus optical power is very poor at biases close to the punch-through voltage (-13.5, -14.0, and -14.5 V). At these reverse biases, the photocurrent initially increases linearly with optical power but saturates at different optical powers. The optical power at which obvious I_{ph} saturation occurs increases with the reverse bias. For example, at 1.25 dBm optical power, we obtained I_{ph}/I_{ideal} values of 0.007, 0.016, and 0.06 at -13.5, -14 and -14.5 V respectively.

At higher biases (above -18 V), Fig. 4 (a) appears to show I_{ph} increasing linearly with optical power. However, a closer inspection shows that the gradient decreases slightly with reverse bias. This can be more easily observed by plotting gain versus optical power as a function of reverse bias, as shown in Fig. 4 (b). As reverse bias and hence the avalanche gain increases, the photocurrent attenuation at high optical power becomes more pronounced. This deviates from the desired APD characteristics where the gain is constant with optical power.

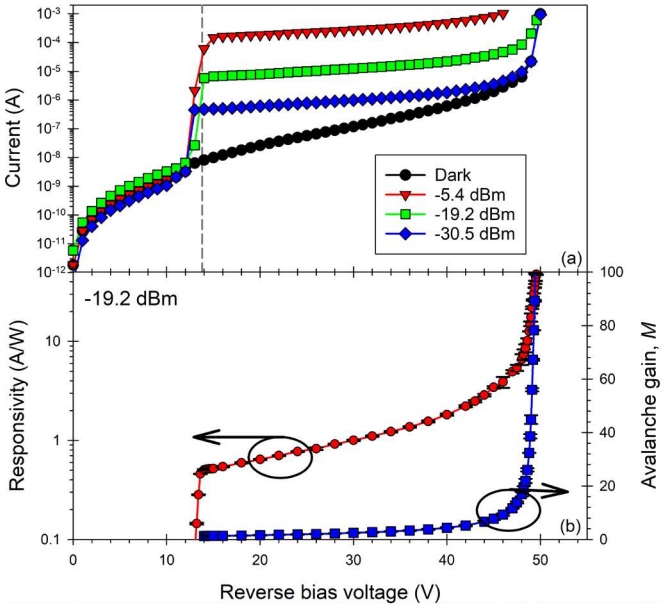

Fig. 3. (a) Dark current of 200 µm diameter device and its photocurrent under 1550 nm wavelength illumination. (b) Mean Responsivity and avalanche gain from three 200 µm diameter APDs under 1550 nm wavelength illumination.

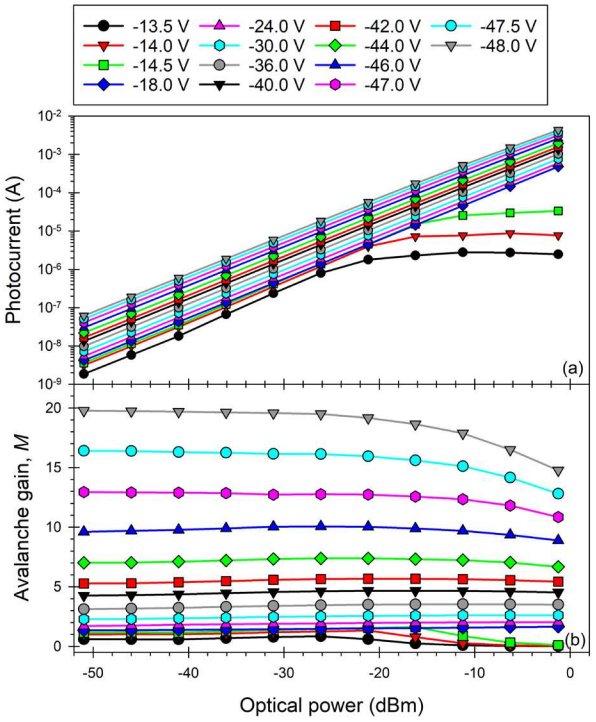

Fig. 4. (a) Experimental output photocurrent and (b) avalanche gain versus optical power on a 200 µm diameter device under various bias voltages.

To observe the dependence(s) of photocurrent attenuation on optical power, reverse bias, and avalanche gain, Fig. 5 (a) shows the ratio of experimental photocurrent to ideal photocurrent, I_{ph}/I_{ideal} versus optical power for four reverse biases. At the highest optical power of -1.25 dBm, as reverse bias increases from -18 to -48 V (corresponding to M =1.5 to 19.6), the I_{ph}/I_{ideal} ratio reduces from 1.0 to 0.77. For comparison, the measurements were repeated on a commercial near-infrared APD with a 200 µm active diameter, IAG-200X [22]. The IAG-200X APD data of I_{ph}/I_{ideal} versus output photocurrent at M =10 is compared with the AlGaAsSb APD data in Fig. 5 (b). For photocurrent beyond 2 µA, the IGA-200X APD photocurrent suffered increasing attenuation such that there is a 10% reduction at ~ 34 µA. In contrast, the AlGaAsSb APD photocurrent reached a 10 % reduction when the photocurrent exceeds 670 µA, ~ 20 times higher.

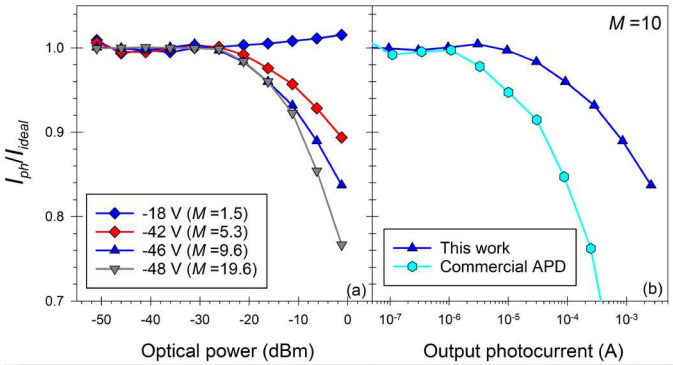

Fig. 5. (a) Ratio of experimental and ideal photocurrent of the AlGaAsSb APD at various bias voltages. (b) Comparison of ratios of experimental and ideal photocurrent at M = 10 for the AlGaAsSb APD and a 200 µm diameter commercial APD [22].

IV. Discussion

When reverse-biased at below or around the punch-through voltage, the AlGaAsSb APD exhibits very poor linearity of photocurrent versus optical power (Fig. 4). This behavior is attributed to energy barriers encountered by electrons travelling from the absorber to the avalanche layer. The band diagrams of our SAM-APD are illustrated in Fig. 1 (b). At 0 V, photogenerated electrons diffusing from the GaAsSb absorber towards the AlGaAsSb avalanche layer face an energy barrier, which many of them are unable to overcome. This remains true until the reverse bias voltage reaches or exceeds the SAM-APD's punch-through voltage (-14 V in this work) when the conduction band is sufficiently tilted so that the larger bandgap layers no longer present as significant energy barriers to the electrons. Hence, many of the photogenerated electrons can drift from the GaAsSb absorber to the AlGaAsSb multiplication layer, improving the linearity of photocurrent versus optical power characteristics significantly.

When reverse-biased at well above the punch-through voltage, the APD's linearity is considerably better compared to when the reverse bias is close to, or below, the punch-through voltage. The difference in linearity performance can be understood by considering the APD electric field profile over the depletion region, $E(y)$, described by Poisson's equation,

$$\frac{dE(y)}{dy} = \frac{q}{\epsilon}(p - n + N_d - N_a), \qquad (1)$$

where q is the electron charge, ε is the permittivity of the material, p is the free hole concentration, n is the free electron concentration, N_d is the donor concentration and N_a is the acceptor concentration. Eqn. (1) assumes complete ionization of the dopant atoms.

At bias voltages just above the punch-through voltage (e.g. -14.5 V in Fig. 4 (b)), the APD has a relatively low electric field in the GaAsSb absorber, as illustrated in Fig. 6 (a). As the optical signal power increases, more photogenerated electrons accumulate at the GaAsSb absorber - AlGaAsSb charge sheet interface because of the energy barrier illustrated in Fig. 1 (b). This leads to increased overall charge density in the charge sheet layer and reduced depletion in the GaAsSb absorber. The overall effect is increased loss of photogenerated electrons to recombination, hence a reduction of photocurrent from the ideal value.

Increasing the reverse bias to well above the punch-through voltage (e.g. -18 V in Fig. 4 (b)) helps to reduce the energy barrier experienced by the accumulated photogenerated electrons, improving the linearity of photocurrent versus optical power characteristics. Thus, the gain appears to be independent of the optical power up to ~ -44 V reverse bias (corresponding gain < 7), as observed in Fig. 4 (b).

Further increase in reverse bias (e.g. -46 to -48 V in Fig. 4 (b)) increases the avalanche gains rapidly. The combination of large avalanche gain and high optical signal power produces high concentrations of free electrons and holes in the avalanche region, as shown in Fig. 6 (b). These carriers create an electric field that opposes the applied electric field, effectively reducing the electric field in the avalanche region and the avalanche gain.

These three distinct ranges of APD linearity behaviors are associated with reverse bias and avalanche gain. Our identification and explanations are not limited to AlGaAsSb-based APDs. They apply to SAM-APDs utilizing different materials for the absorber and the avalanche region. This work utilizes the AlGaAsSb avalanche region to exploit the excellent temperature stability offered by AlGaAsSb. For SAM-APDs using other avalanche materials whose avalanche gains are more sensitive to temperature variations, their linearity of photocurrent versus optical signal power at high gains is likely to be worse, when compared to AlGaAsSb-based APDs.

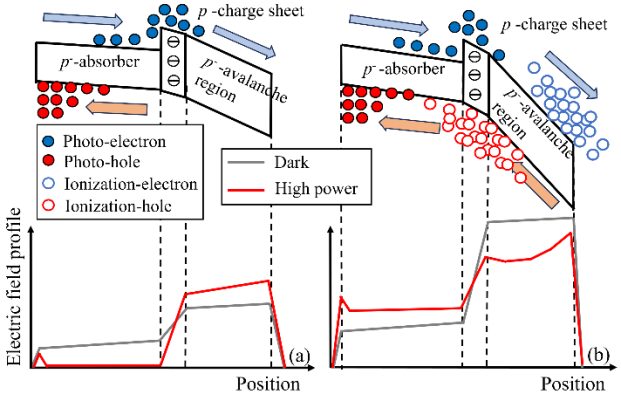

Fig. 6. Schematic band diagrams and electric field profiles for a SAM-APD designed for pure electron injection under high optical power illumination, when the APD is reverse-biased at (a) around its punch-through voltage (low or moderate gains) and (b) close to its breakdown voltage (high gains).

V. Conclusion

We have studied the linearity performance of a near-infrared SAM-APD utilizing the AlGaAsSb avalanche layer. The thin AlGaAsSb avalanche layer minimizes any effect(s) of APD gain dependence on temperature. The photocurrent versus optical signal power measurements were carried out over a wide range of optical signal power, reverse bias, and avalanche gain. Different linearity behaviors were identified from three ranges of reverse bias and avalanche gain.

Around the punch-through voltage, linearity is poor because the optical signal power directly affects the number of photogenerated electrons accumulating at the absorber–charge sheet interface, which in turn changes the depleted portion of the absorber. At higher reverse bias and moderate gains, the accumulation of photogenerated electrons at the absorber–charge sheet interface is less significant; hence photocurrent increases linearly with optical power. At reverse bias close to the breakdown voltage, the avalanche gains are large so there are high concentrations of free electrons and holes in the avalanche region if high optical signal power is used. The opposing electric field from these free carriers reduces the applied electric field in the avalanche region and hence the avalanche gain, degrading linearity performance. Our findings of linearity performance apply to SAM-APDs beyond those with AlGaAsSb avalanche regions.

Finally, SAM-APDs with AlGaAsSb avalanche regions exhibit better linearity performance compared to commercial non-AlGaAsSb SAM-APD. The optical power at which 10 % attenuation in photocurrent occurs at the output photocurrent of 670 µA in the former and 34 µA in the latter at M =10. Hence AlGaAsSb SAM-APDs are promising detectors for optical communication links utilizing high-order signal modulation formats.

References

[1] M. Nada, T. Hoshi, H. Yamazaki, T. Hashimoto, and H. Matsuzaki, "Linearity improvement of high-speed avalanche photodiodes using thin depleted absorber operating with higher order modulation format," *Opt Express*, vol. 23, no. 21, p. 27715, Oct. 2015, doi: 10.1364/oe.23.027715.

[2] T. Kobayashi, F. Hamaoka, M. Nakamura, H. Yamazaki, M. Nagatani, and Y. Miyamoto, "Ultrahigh-speed optical communications technology combining digital signal processing and circuit technology," *NTT Technical Review*, vol. 17, no. 5, 2019, doi: 10.53829/ntr201905fa2.

[3] V. J. Urick, J. D. Mckinney, and K. J. Williams, *Fundamentals of microwave photonics*. 2015. doi: 10.1002/9781119029816.

[4] M. Nada, Y. Yamada, and H. Matsuzaki, "A High-Linearity Avalanche Photodiodes With a Dual-Carrier Injection Structure," *IEEE Photonics Technology Letters*, vol. 29, no. 21, pp. 1828–1831, Nov. 2017, doi: 10.1109/LPT.2017.2753262.

[5] H. Xing, J. Zhang, A. Liu, and Y. Yang, "Design of high linearity InGaAs/InP avalanche photodiode with a hybrid absorption layer structure," *Infrared Phys Technol*, vol. 102, Nov. 2019, doi: 10.1016/j.infrared.2019.103018.

[6] Y. Jiang and J. Chen, "Optimization of the Linearity of InGaAs/InAlAs SAGCM APDs," *Journal of Lightwave Technology*, vol. 37, no. 14, pp. 3459–3464, Jul. 2019, doi: 10.1109/JLT.2019.2917262.

[7] D. S. Ong, K. F. Li, G. J. Rees, J. P. R. David, and P. N. Robson, "A simple model to determine multiplication and noise in avalanche photodiodes," *J Appl Phys*, vol. 83, no. 6, 1998, doi: 10.1063/1.367111.

[8] S. A. Plimmer, J. P. R. David, D. S. Ong, and K. F. Li, "A simple model for avalanche multiplication including deadspace effects," *IEEE Trans Electron Devices*, vol. 46, no. 4, pp. 769–775, 1999, doi: 10.1109/16.753712.

[9] M. M. Hayat and G. Dong, "A new approach for computing the bandwidth statistics of avalanche photodiodes," *IEEE Trans Electron Devices*, vol. 47, no. 6, 2000, doi: 10.1109/16.842973.

[10] Y. Cao, T. Blain, J. D. Taylor-Mew, L. Li, J. S. Ng, and C. H. Tan, "Extremely low excess noise avalanche photodiode with GaAsSb absorption region and AlGaAsSb avalanche region," *Appl Phys Lett*, vol. 122, no. 5, p. 051103, Jan. 2023, doi: 10.1063/5.0139495.

[11] S. Lee *et al.*, "High gain, low noise 1550 nm GaAsSb/AlGaAsSb avalanche photodiodes," *Optica*, vol. 10, no. 2, 2023, doi: 10.1364/optica.476963.

[12] X. Collins *et al.*, "Low-noise AlGaAsSb avalanche photodiodes for 1550 nm light detection," SPIE-Intl Soc Optical Eng, Mar. 2023, p. 24. doi: 10.1117/12.2651669.

[13] Phlux Technology, "Aura Series-200 µm Datasheet." Accessed: Mar. 05, 2024. [Online]. Available: https://phluxtechnology.com/assets/general/phlux-aura-datasheet-200um_2024-01-24-130418_okts.pdf

[14] Y. Cao, T. Osman, E. Clarke, P. K. Patil, J. S. Ng, and C. H. Tan, "A GaAsSb/AlGaAsSb Avalanche Photodiode With a Very Small Temperature Coefficient of Breakdown Voltage," *Journal of Lightwave Technology*, vol. 40, no. 14, pp. 4709–4713, Jul. 2022, doi: 10.1109/JLT.2022.3167268.

[15] K. S. Hyun and C. Y. Park, "Breakdown characteristics in InP/InGaAs avalanche photodiode with p-i-n multiplication layer structure," *J Appl Phys*, vol. 81, no. 2, pp. 974–984, 1997, doi: 10.1063/1.364225.

[16] L. E. Tarof, "Planar InP-InGaAs Avalanche Photodetectors with n-Multiplication Layer Exhibiting a Very High Gain-Bandwidth Product," *IEEE Photonics Technology Letters*, vol. 2, no. 9, 1990, doi: 10.1109/68.59337.

[17] L. Juen *et al.*, "Temperature Dependence of Avalanche Breakdown in InP and InAlAs," *IEEE J Quantum Electron*, vol. 46, no. 8, pp. 1153–1157, 2010.

[18] B. F. Levine *et al.*, "A new planar InGaAs-InAlAs avalanche photodiode," *IEEE Photonics Technology Letters*, vol. 18, no. 18, 2006, doi: 10.1109/LPT.2006.881684.

[19] D. S. G. Ong, J. S. Ng, Y. L. Goh, C. H. Tan, S. Zhang, and J. P. R. David, "InAlAs avalanche photodiode with type-II superlattice absorber for detection beyond 2 µm," *IEEE Trans Electron Devices*, vol. 58, no. 2, pp. 486–489, 2011, doi: 10.1109/TED.2010.2090352.

[20] A. Beling, H. Pan, H. Chen, and J. C. Campbell, "l, 'Measurement and modeling of a high-linearity modified unitraveling carrier photodiode,' IEEE Photonics Technol. Lett. 20(14), 1219–1221 (2008).," *IEEE Photonics Technology Letters*, vol. 20, no. 14, 2008, doi: 10.1109/LPT.2008.926016.

[21] S. Adachi, *Properties of Semiconductor Alloys: Group-IV, III-V and II-VI Semiconductors*. 2009. doi: 10.1002/9780470744383.

[22] LC-APD, "InGaAs Avalanche Photodiode IAG-Series." [Online]. Available: www.lasercomponents.fr